

Phase Incremented Echo Train Acquisition applied to Magnetic Resonance Pore Imaging

S.A. Hertel^{a,1}, P. Galvosas^a

^aMacDiarmid Institute for Advanced Materials and Nanotechnology, School of Chemical and Physical Sciences, Victoria University of Wellington, Wellington 6140, New Zealand

Abstract

Efficient phase cycling schemes remain a challenge for NMR techniques if the pulse sequences involve a large number of rf-pulses. Especially complex is the Carr Purcell Meiboom Gill (CPMG) pulse sequence where the number of rf-pulses can range from hundreds to several thousands. Our recent implementation of Magnetic Resonance Pore Imaging (MRPI) is based on a CPMG rf-pulse sequence in order to refocus the effect of internal gradients inherent in porous media. While the spin dynamics for spin-1/2 systems in CPMG like experiments are well understood it is still not straight forward to separate the desired pathway from the spectrum of unwanted coherence pathways. In this contribution we apply Phase Incremented Echo Train Acquisition (PIETA) to MRPI. We show how PIETA offers a convenient way to implement a working phase cycling scheme and how it allows one to gain deeper insights into the amplitudes of undesired pathways.

1. Introduction

The motion of spin bearing particles can be studied by the judicious use of pulsed magnetic field gradients in NMR experiments [1, 2]. Pulsed Gradient Spin Echo (PGSE) NMR is best known for diffusion measurements in porous media as well as for velocimetry studies [2]. The potential of PGSE NMR for NMR microscopy has been demonstrated with the appearance of diffraction patterns when self-diffusion was studied in a bead pack sample [3]. Magnetic Resonance Pore Imaging (MRPI) is a recent advancement in PGSE NMR which dramatically increases the resolution as compared to MRI for suitable closed pore systems [4]. MRPI relies on a weak gradient pulse which can be several hundreds of milliseconds long. During this gradient pulse the nuclear spins have to be kept in the transverse plane [5, 6]. We suggested therefore a CPMG based design in order to refocus the internal gradients and other experimental imperfections [7, 8]. However, the introduction of many rf-pulses in the presence of magnetic field gradients leads to a complicated coherence pathway spectrum [9, 10]. This may not always be a problem in CPMG relaxation studies, since the decay due to transverse relaxation is still obtained [11]. In MRPI however, it is essential to preserve the spin phase throughout the rf-pulse train, while the unwanted pathways do interfere adversely [8]. Since traditional phase cycling techniques proved impractical for our CPMG pulse sequence design, it was necessary to explore alternative ways to filter for the correctly encoded signal. This study focuses on the application of a novel phase cycling technique called Phase Incremented Echo Train Acquisition (PIETA) [12].

In pulsed NMR the spectrum of coherence pathways (CPs) is multiplied with each additional rf-pulse [13]. This creates

a very rich spectrum of CPs, where each CP contains specific information which is influenced by its history since excitation. Since each coherence may experience different physical interactions, it is paramount to select the right CPs of the spin system under study. The most popular strategy to achieve this selection involves the nested cycling of the rf-pulse phases and the receiver phase from scan to scan according to a master equation [14, 15]. However, the number of CPs grows exponentially with the number of rf-pulses and finding the right phase cycling scheme may become complicated. Throughout the article we consider a spin-1/2 system without coupling between the individual spins and where the desired CP does not involve any z -storage. In this case, an NMR pulse sequence with 10 rf-pulses would need $N = 3^{10} = 59049$ phase steps following the nested phase cycling scheme [16]. Several algorithms were designed to solve this problem with the help of computer programs [17, 18, 19]. Two other widely applied strategies are improved perfection of the spin rotations induced by specially designed rf-pulses [20] and the application of pulsed field gradients [21]. These two latter strategies can reduce the complexity of the problem, but they are often harder to implement or face limitations due to the available hardware. Especially the Carr-Purcell-Meiboom-Gill (CPMG) NMR pulse sequence [22, 23] and its derivatives can contain several hundreds or even thousands of rf-pulses and the number of phase steps with traditional phase cycling would be forbiddingly high. A first solution emerged with the development of Cogwheel phase cycling which when applied to CPMG like pulse trains promised significant reductions in the number of phase steps needed [24]. When Cogwheel is applied to CPMG the receiver phases have to be cycled such that they span a 2π angle range after n_{rf} acquisitions, where n_{rf} is the number of 180° rf-pulses [24]. This renders this method appealing for experiments with a fixed number of rf-pulses. However, in the case of CPMG echo trains with a variable number of rf-pulses it would require as many

Email address: stefan.hertel@shell.com (S.A. Hertel)

¹Currently at Shell Intl. E&P Inc., Rock and Fluid Physics, Houston, TX

independent measurements (including the Cogwheel phase cycle) as different numbers of rf-pulses have been chosen. A recent approach called Phase Incremented Echo Train Acquisition (PIETA) offers the extraction of all echoes in a given rf-pulse train and a de-convolution of the contributing coherence pathways with the same number of scans as Cogwheel [12].

In this work, PIETA is utilized to investigate the coherence pathway spectrum contributing to the spin echo signal of MRPI. Furthermore, it is shown how the artifact free coherence pathway can be selected.

2. Theory

2.1. Phase cycling

In NMR experiments the desired information is usually contained in one specific coherence pathway (CP) $\mathbf{p} = (p_0, p_1, p_2, \dots, p_n)$ or a small subset \mathcal{P} of all CPs [25]. The values p_k denote the coherence order of the spins after the k -th rf-pulse of the NMR pulse sequence. The elements p_k can assume integer values which are determined by the spin quantum number I and the coupling between multiple spins. For a system of uncoupled spin-1/2 nuclei the values of p_k can be $+1, -1$ and 0 . It is assumed that every CP starts from a well defined equilibrium with $p_0 = 0$ (associated with magnetization in z -direction) before the first rf-pulse. For a CP to be measured with quadrature NMR detection it has to end with $p_n = -1$ [25]. The magnetization of all three levels $\{+1, -1, 0\}$ is mixed with each additional rf-pulse giving rise to a large number of CPs growing exponentially with 3^n , where n is the number of rf-pulses [11]. The complex NMR signal for a single scan with scan counter m can be expressed as

$$s_m(t) = \sum_{\mathbf{p}} s_{\mathbf{p}}(t) \exp\{-i \phi_{\mathbf{p}}(m)\}, \quad (1)$$

where $s_{\mathbf{p}}(t)$ is the signal arising from a specific coherence pathway \mathbf{p} after the last rf-pulse. $\phi_{\mathbf{p}}(m)$ denotes the final phase with which the CP is recorded in the spectrometer memory and it is given by [24]

$$\phi_{\mathbf{p}}(m) = \Delta p_1 \phi_1(m) + \Delta p_2 \phi_2(m) + \dots + \Delta p_n \phi_n(m) + \phi_{\text{rec}}(m). \quad (2)$$

Here, ϕ_k are the phases of the k -th rf-pulse and $\Delta p_k = p_k - p_{k-1}$ is the coherence transfer difference induced with the k -th rf-pulse. The signal after N scans can be expressed as the complex sum given by

$$\begin{aligned} s(t) &= \sum_{m=1}^N s_m(t) \\ &= \sum_{m=1}^N \sum_{\mathbf{p}} s_{\mathbf{p}}(t) \exp\{-i \phi_{\mathbf{p}}(m)\} \\ &= \sum_{\mathbf{p}} s_{\mathbf{p}}(t) \sum_{m=1}^N \exp\{-i \phi_{\mathbf{p}}(m)\}, \end{aligned} \quad (3)$$

where we inserted eq. 1 in the first step and in the second step we used the fact that $s_{\mathbf{p}}(t)$ does not depend on m . The last term in eq. 3 shows that each individual CP signal is multiplied by the sum of phase factors added over all N scans. Thus, in order to filter any desired pathway \mathbf{p} after N scans, the following condition has to be full-filled

$$\sum_{m=1}^N \exp\{-i \phi_{\mathbf{p}}(m)\} = \begin{cases} N & \text{if } \mathbf{p} \in \mathcal{P} \\ 0 & \text{otherwise.} \end{cases} \quad (4)$$

The most popular strategies to achieve this condition are the nested phase cycling approach [14, 15] and Cogwheel phase cycling scheme [24]. Both methods involve the design of a set of $\phi_k(m)$ for each scan m and to cycle the receiver phase ϕ_{rec} such that the wanted CP is always recorded with the same phase, while all other CPs cycle in phase and cancel upon completion of the full set of scans. In the case of many rf-pulses, such as they are common in CPMG type experiments, these methods are hard to apply because of the sheer number of CPs and they do not provide any extra information about the importance of the unwanted CPs.

A different concept was proposed with Multiplex phase cycling [26] where each scan is recorded separately in the spectrometer memory and the wanted CPs are selected in a post-processing step. It will be shown in the next section how PIETA is similar to both multiplexing and Cogwheel phase cycling.

2.2. Phase Incremented Echo Train Acquisition

Baltisberger et al. [12] introduced a new phase cycling scheme which allows one to extract the direct CP from Echo Train Acquisition (ETA) experiments. The authors use ETA as a general expression for a train of spin echos due to a train of rf-pulses, which can be appended to an NMR experiment or may represent a stand-alone experiment like CPMG. This novel approach was called Phase Incremented Echo Train Acquisition (PIETA), because the phase of every other refocusing pulse is incremented as a single variable $\phi_{\mathbf{p}}$ from scan to scan. Note that the application of PIETA in this contribution slightly deviates from the use cases suggested by Baltisberger *et. al* [12]. Instead of recording many spin echo amplitudes for each scan, here only one spin echo is recorded at the end of the rf-pulse train for each scan as will be explained below. PIETA applied to the CPMG pulse sequence is shown in fig. 1. The part enclosed by the dashed line is repeated multiple times to create a train of refocusing 180° rf-pulses. The rf-pulse phase $\phi_{\mathbf{p}}$ is incremented from scan to scan, while the phases of the leading 90° rf-pulse, of every other 180° rf-pulse and of the receiver phase ϕ_{rec} stay fixed for all scans. The level diagram below the rf-pulses in fig. 1 shows the three coherence orders $0, +1, -1$. In this level diagram the direct CP which is measured for even echos $\mathbf{p} = (0, -1, +1, -1, \dots, +1, -1)$ is indicated as a solid line, while its conjugate for the odd echos $\tilde{\mathbf{p}} = (0, +1, -1, +1, -1, \dots, +1, -1)$ is shown as a dashed line. With PIETA the vector of spectrometer phases for the m -th scan is given by $\boldsymbol{\phi}(m) = (\phi_1 = 0, \phi_{\mathbf{p}} = \nu m, \phi_3 = \pi/2, \phi_{\mathbf{p}} = \nu m, \dots, \phi_{\text{rec}} = 0)$, where ν is a winding number given by

$$\nu = \frac{2\pi}{N}. \quad (5)$$

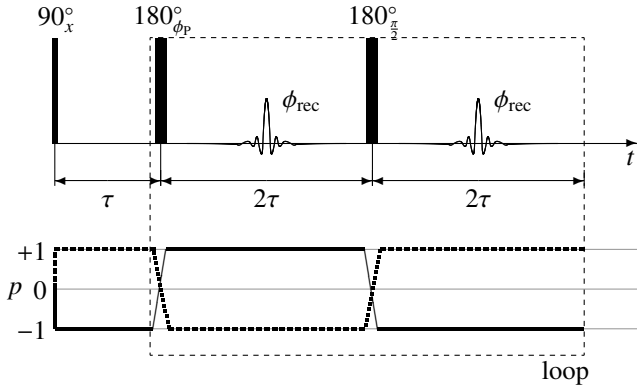


Figure 1: PIETA phase scheme as applied to the CPMG pulse sequence, where every second 180° rf-pulse is phase incremented with the rf-pulse phase ϕ_p . The phases of the 90° rf-pulse and every even 180° rf-pulse as well as the receiver phase ϕ_{rec} stay fixed.

Thus, the phase ϕ_p is rotated by 2π when all N scans are completed. The final signal phase for the PIETA experiment as shown in fig. 1 is given by

$$\phi_p(m) = vm\Delta p_2 + vm\Delta p_4 + \dots \quad (6)$$

where the phases which remain fixed for all scans have been neglected. The fixed phases lead to a constant phase for all scans and will not be needed in the following analysis. One may write eq. 6 as a sum leading to

$$\begin{aligned} \phi_p(m) &= vm \sum_{k \text{ even}} \Delta p_k \\ &= vm\Delta P, \end{aligned} \quad (7)$$

where ΔP is defined as the cumulative coherence transfer difference induced by the even rf-pulses ($\Delta P = \sum_{k \text{ even}} \Delta p_k$) which are phase cycled with ϕ_p . Therefore, the NMR signal as given by eq. 1 can be rewritten according to

$$s_m(t) = \sum_p s_p(t) \exp\{-i vm\Delta P\}. \quad (8)$$

It can be seen that ΔP assumes the role of a modulation frequency when the signal is acquired as a function of the phase $\phi_p = vm$.

Similar to the multiplex phase cycling scheme [26], all the spin echos in the CPMG train are stored separately for each scan in the computer memory, while ϕ_p is incremented from scan to scan. Let the number of spin echos recorded be denoted by n_E then the stored data is the signal matrix $s(n_E, t, \phi_p)$. In this matrix, t represents the discrete time steps which start all over again with each spin echo n_E . One may recall that ϕ_p is connected with ΔP as the underlying modulation frequency (see eq. 7) which implies that $s(n_E, t, \Delta P)$ and $s(n_E, t, \phi_p)$ are a Fourier pair similar to the relation found in [27]. Thus, after all scans are completed one can perform a discrete Fourier transform in the ϕ_p direction of the data matrix to obtain the signal in the ΔP dimension according to

$$\begin{aligned} s(n_E, t, \Delta P) &= \mathcal{F}\{s(n_E, t, \phi_p)\} \\ &= \int s(n_E, t, \phi_p) \exp\{-i \phi_p \Delta P\} d\phi_p. \end{aligned} \quad (9)$$

The crucial observation of Baltisberger et al.[12] is that ΔP is unique for the direct CP and can be extracted from $s(n_E, t, \Delta P)$ without interference of any other CPs.

For the isolated spin-1/2 system considered here, the direct CP difference vector for even n_E is given by $\Delta \mathbf{p} = (-1, +2, -2, \dots, +2)$ and for odd n_E is given by $\Delta \mathbf{p} = (+1, -2, +2, \dots, -2)$. The CP difference for each rf-pulse cycled with ϕ_p is equal to $\Delta p_k = +2$, while for odd spin echos it is equal to $\Delta p_k = -2$ since the conjugate CP $\tilde{\mathbf{p}}$ is measured. All other CP vectors have one or more elements with $|\Delta p_k| < 2$ and thus they have a smaller cumulative coherence pathway difference ΔP .

ΔP for the direct coherence pathway in dependence of the spin echo count is given by [28]

$$\Delta P = (-1)^{n_E} \left\{ 2 \left\lfloor \frac{n_E - 1}{2} \right\rfloor + 2 \right\}, \quad (10)$$

where $\lfloor x \rfloor$ is the integer floor function. Note that for CPMG the spin echo count as a function of the number of rf-pulses n is given by $n_E = n - 1$ in order to account for the 90° excitation pulse.

There is a minimum number of scans needed in order to completely de-alias the direct CP, since the number of phase increments has to be chosen such that the Nyquist-Shannon criterion [29] is full-filled. In the case of PIETA the sampling frequency is given by $\nu = 2\pi/N$. This frequency has to be at least double the frequency which shall be detected. The highest frequency to be detected is given by $\Delta P(n_E)$ for the direct CP as given by eq. 10. Thus, if the spin echo count is even then $\Delta P = n_E$ and for odd spin echos it is $\Delta P = -(n_E + 1)$. Therefore, the number of phase increments in dependence on the echo count is given by

$$N \geq \begin{cases} 2n_E & \text{if } n_E \text{ even} \\ 2(n_E + 1) & \text{if } n_E \text{ odd.} \end{cases} \quad (11)$$

In this work, the spin echo count n_E will not be increased as compared to conventional CPMG relaxation experiments. Instead, n_E stays fixed and the gradient amplitude is stepped as will be explained in the next section.

2.3. Magnetic Resonance Pore Imaging

Magnetic Resonance Pore Imaging (MRPI) can be regarded as a Pulsed Gradient Spin Echo (PGSE) NMR technique. PGSE NMR techniques measure the NMR signal as a function of the wave vector $\mathbf{q} = \gamma\delta\mathbf{G}/2\pi$, where \mathbf{G} denotes the gradient amplitude, γ is the gyro-magnetic ratio of the observed nucleus and δ is the length of the gradient pulses. The PGSE NMR signal is usually normalized with the NMR signal obtained with zero gradient pulse amplitude $E(\mathbf{q}) = M(\mathbf{q})/M(\mathbf{q} = 0)$. Recently, Laun *et al.* [4] suggested the gradient pulse pattern used for MRPI, which created a hybrid between MRI and PGSE NMR. With MRPI the spin echo attenuation is resembling the averaged form factor $\overline{S}_0(\mathbf{q})$ of the pores as measured in the direction of \mathbf{q} . The form factor is the Fourier transform of the pore shape $\rho_0(\mathbf{r})$. Therefore, one may obtain an average image of the pores by performing an inverse Fourier transformation of

the MRPI spin echo attenuation if certain requirements are met, i.e. $\overline{\rho_0(\mathbf{r})} = \mathcal{F}^{-1}\{\overline{S_0(\mathbf{q})}\}$. Note that the pore shape $\rho_0(\mathbf{r})$ equals the spin density distribution if the spin density is homogeneous throughout the pore space. In this contribution we discuss the experimental results for a cylindrical capillary sample for which the form factor is given by

$$S_0(\mathbf{q}) = \frac{J_1(2\pi qL)}{\pi qL}, \quad (12)$$

where J_1 denotes the cylindrical Bessel function of first order and L is the radius of the cylindrical domain. For obtaining eq. 12 the wave-vector \mathbf{q} has to be applied perpendicular to the cylinder axis. In the following discussion it will be assumed that the gradient pulses will always be applied in this direction and therefore the vector notation is dropped.

MRPI relies on the application of a long gradient pulse with duration δ_L and amplitude G_L as shown in fig. 2 (a). The long gradient pulse allows for diffusion encoding, while the intense gradient with amplitude G_N and duration δ_N acts similar to a phase imaging gradient in MRI [4]. These two gradient pulses have to full-fill the spin echo condition $\int_0^T G^*(t) dt = 0$ which requires $G_L\delta_L = G_N\delta_N$. Here, T is defined as the time from the onset of the first gradient pulse until the end of the last gradient pulse. Fig. 2 (b) shows schematically the replacement of

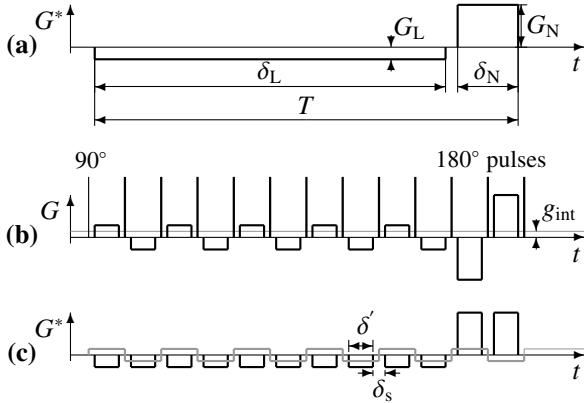


Figure 2: Gradient pulse pattern of the MRPI pulse sequence as proposed by Laun et. al [4] (a). The presence of a constant internal gradient g_{int} (grey) required the replacement used for this work which consisted of a sequence of gradient pulses interspersed with 180° rf-pulses (b). The pulsed gradients effectively add up, while the internal gradient g_{int} is compensated (c).

the gradient pulse pattern as initially suggested in [4] with the one used in this work. The gradient pulses were applied with alternating polarity in the laboratory reference frame while they were interspersed with 180° rf-pulses. The replacement was chosen to minimize the dephasing due to the internal gradients g_{int} by refocusing their influence on the spin phases [7]. Fig. 2 (c) shows the effective gradient pattern $G^*(t)$ as experienced by the spin system when the effect of the 180° pulses is accounted for. The pulsed gradients are effectively adding up to yield a pattern similar to fig. 2 (a), while the internal gradients are compensated. Note that many more gradient pulses were used in the actual implementation, which will be shown in sec. 3 along with the rf-pulse phases.

For illustration purposes, consider the gradient pattern as shown in fig. 2 (a). In the ideal case that the weak gradient pulse is infinitely long and the intense pulse is applied instantaneously the spin echo attenuation is given by [4]

$$E(q | \delta_L \rightarrow \infty, \delta_N \rightarrow 0) = \overline{S_0(q)}, \quad (13)$$

which yields the form factor $\overline{S_0(q)}$ averaged over the pores in the sample. Under experimental conditions the requirements $\delta_L \rightarrow \infty$ and $\delta_N \rightarrow 0$ cannot be full-filled. Fortunately, the need for infinitely long gradient pulses can be relaxed to the condition that the molecules traverse the pore space multiple times such that $D\delta_L \gg L^2$. However, this less stringent requirement has been linked to blurring of the obtained average pore image [5, 8]. Secondly, the diffusion encoding during δ_N has to be accounted for as well, since the intense gradient pulse cannot be applied instantaneously. On average the molecules push away from the pore walls during δ_N , which leads to edge enhancement similar to the phenomenon in MRI [5, 8]. These two effects together with experimental adaptations of MRPI may pose challenges for the formulation of fitting functions especially when the gradient pattern involves many pulses as shown in fig. 2 (b) and (c). Therefore, the Multiple Correlation Function (MCF) technique was employed for the simulation of the spin echo decay. This simulation technique is flexible enough for most gradient pulse patterns and it can adequately account for both blurring and edge enhancement [30].

In MCF the PGSE NMR signal is found by evaluating the ordered matrix product

$$E \approx \left[\prod_{k=1}^K \exp[-(p\Lambda + i q_G f(k\tau)\mathcal{B})\tau/T] \right]_{0,0}, \quad (14)$$

where $[\dots]_{0,0}$ denotes the first diagonal element of the resulting matrix. The piece-wise constant function $f(k\tau)$ is the dimensionless temporal profile of the normalized spatial magnetic field profile $\tilde{B}(\mathbf{r})$ with maximum amplitude β , such that the magnetic field at any time t is given by

$$B(\mathbf{r}, k\tau) = f(k\tau)\beta\tilde{B}(\mathbf{r}). \quad (15)$$

\mathcal{B} is the correlation matrix of the spatial gradient profile $\tilde{B}(\mathbf{r})$ with the eigenfunctions of the Laplace operator and Λ is the diagonal eigenvalue matrix of the Laplace operator. Furthermore, $p = DT/L^2$ is the reduced self-diffusion coefficient and $q_G = \gamma\beta TL$ denotes the generalized gradient intensity. More detailed descriptions of the MCF technique and its application to MRPI can be found in [5, 8].

For calibration purposes the spin echo decay has been measured previously in an isotropic liquid [8]. When MRPI is applied to nuclear spins in an isotropic unrestricted liquid one obtains a Gaussian attenuation similar to other PGSE NMR techniques given by

$$E(q) = \exp\{-D(2\pi q)^2 \Delta_{\text{eff}}\}, \quad (16)$$

where D is the self-diffusion coefficient of the spin bearing molecules and Δ_{eff} is the effective observation time, which is

a function of the pulsed gradient pattern $G(t)$. In the NMR self-diffusion literature, the term $(2\pi q)^2 \Delta_{\text{eff}}$ is usually captured as one variable in the so called b -factor [31]. However, in this contribution the case of unrestricted self-diffusion will be compared to the case of q -space imaging with MRPI. Therefore, we chose to express the spin echo attenuation as a function of the q -value. The effective diffusion time Δ_{eff} can be calculated in analogy to the well known double integral for the calculation of the b -factor in the PGSE NMR literature [1, 31]. It is given by

$$\Delta_{\text{eff}} = \frac{1}{(2\delta')^2} \int_0^t dt' \left[\int_0^{t'} dt'' f(t'') \right]^2, \quad (17)$$

where the factor $1/(2\delta')^2$ is appearing, because it has been factored into the q -value which is given by $q = \gamma 2\delta' G_N / 2\pi$ for our implementation. For this work, only two intense gradient pulses were applied and N_L gradient pulses are adding up to yield the weak long gradient. Evaluation of eq. 17 for the CPMG based MRPI pulse sequence as shown in fig. 2 (c) yields [8]

$$\Delta_{\text{eff}} = \frac{1}{3} \left[\delta' (N_L + 2) + \delta_s \left(\frac{2N_L^2 + 3N_L + 1}{2N_L} + \frac{3}{4} \right) \right], \quad (18)$$

where δ' is the gradient pulse duration and where δ_s is the separation between the gradient pulses, i.e. the time from the end of one gradient pulse until the leading edge of the next gradient pulse.

3. Experimental parameters and samples

3.1. Pulse sequence design

Figure 3 a) shows the rf-pulse sequence of the CPMG based MRPI experiment [7, 8]. The rf-pulse phases were implemented

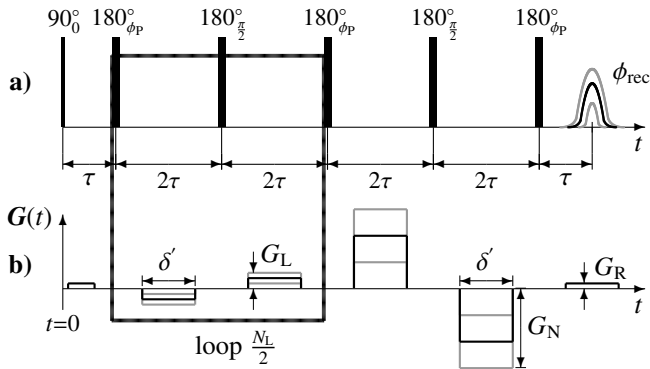


Figure 3: MRPI pulse sequence with a CPMG like rf-pulse scheme (a). The long gradient is replaced by N_L gradient pieces with gradient amplitude G_L and the narrow gradient pulse is split into two intense gradient pulses with gradient amplitude G_N . The gradients are shown relative to each other as applied in the laboratory reference frame ($G(t)$) (b). Effectively, the gradient pulses G_L add up and are balanced by the two gradient pulses G_N . In practice the gradient pulses are ramped in order to reduce eddy currents (not shown).

according to the PIETA phase scheme, where the odd 180° rf-pulses are phase cycled with ϕ_p . The phase in units of radians

of the 90° rf-pulse was fixed at 0, the phases of the even numbered 180° rf-pulse were set to $\pi/2$ and the receiver phase ϕ_{rec} was kept at 0. The gradient pulse scheme $G(t)$ is depicted in fig. 3 b). Here, $G(t)$ shows the relative amplitude of the gradient pulses as they are applied in the laboratory reference frame. There is a read gradient G_R applied in the beginning of the pulse sequence and during the detection period for the detection of gradient pulse mismatches. For this study, the number of long gradient pulses with amplitude G_L ranged from $N_L = 30$ to $N_L = 50$. Note that no spin echo is formed until after the last 180° rf-pulse. Thus, the spin echo count is fixed and for the implementation shown in fig. 3 it is given by $n_E = N_L + 3$. Considering eq. 10 and the fact that n_E is an odd number it follows that the desired signal is contained in the matrix elements of $s(q, t, \Delta P)$ where $\Delta P = -(n_E + 1) = -(N_L + 4)$.

Previous MRPI results as discussed in [7] and [8] have been obtained with the same pulse sequence, but with a 4-step phase cycle. Table 1 shows the phase cycle, which has been designed in analogy to a cyclops phase cycle adapted to the special case of the MRPI pulse sequence. The rf-pulse phases are not shown

Pulse phases				
ϕ_{90}	ϕ_{odd}	ϕ_{even}	ϕ_{last}	ϕ_{rec}
0	0	π	$\frac{\pi}{2}$	π
0	$\frac{\pi}{2}$	$\frac{3\pi}{2}$	0	0
0	π	0	$\frac{3\pi}{2}$	π
0	$\frac{3\pi}{2}$	$\frac{\pi}{2}$	π	0

Table 1: Phase cycle of the CPMG based MRPI pulse sequence with 4 phase steps. The rf-phases ϕ_{odd} correspond to the odd numbered 180° rf-pulses in fig. 3 (a), while ϕ_{even} is the phase applied for the even numbered 180° rf-pulses. The last 180° pulse has a separate phase ϕ_{last} assigned.

in fig. 3, but have been named ϕ_{odd} for the odd 180° rf-pulses, ϕ_{even} for the even 180° rf-pulses and ϕ_{last} for the last 180° rf-pulse before detection. The rf-pulse phase ϕ_{last} has been introduced to filter the pathway $p = 0, +1, 0, \dots, 0, -1$, which does not experience the stepped gradient pulses and can therefore not be dephased.

3.2. Hardware and samples

The experiments were carried out on a Bruker Avance II spectrometer with a proton resonance frequency of 400 MHz. The gradient pulses were generated by a Bruker GREAT 60 gradient amplifier in conjunction with a Micro 2.5 imaging probe. At maximum current output of 60 A the gradient system provided gradient strengths up to $G_{\text{max}} = \pm 1.45 \text{ Tm}^{-1}$. The utilized rf-coil had a birdcage coil design with an inner diameter of $ID = 1 \text{ cm}$. Typical rf-pulse durations were $t_{90^\circ} = 12.5 \mu\text{s}$ and $t_{180^\circ} = 25 \mu\text{s}$ when utilizing ^1H as the NMR active nuclei.

A spherical sample tube ($OD = 1 \text{ cm}$) filled with CuSO_4 doped H_2O was utilized for testing of the MRPI pulse sequence and to measure the spin echo attenuation for unrestricted self-diffusion. For the MRPI experiments in a model porous system a capillary sample was prepared, which contained ca. 470 polyimide coated glass capillaries with inner diameter of $d =$

$20 \pm 2 \mu\text{m}$. These capillaries were filled with distilled H_2O according to the procedure outlined in [8].

4. Results

It has been shown previously that the MRPI pulse sequence can be calibrated by measuring the free self-diffusion coefficient D of a suitable isotropic liquid [8]. Thus, the CPMG based MRPI pulse sequence was applied to the spherical H_2O sample described in sec. 3.2 and the PIETA phase cycle was applied to investigate the coherence pathway spectrum. The number of long gradient pulses was $N_L = 50$, which were refocused by $N_N = 2$ narrow gradient pulses. The measured spin echo corresponds to the spin echo count $n_E = 53$ and therefore the number of phase steps was set to $N = 128$, respecting the condition of eq. 11. The resulting data matrix $s(q, t, \phi_p)$ had dimensions of $32 \times 512 \times 128$, where q was incremented in 32 steps, 512 points were acquired in the time domain for each scan and 128 phase steps were acquired. A subsequent Fourier transform analogous to eq. 9 in the ϕ_p direction yielded the signal matrix $s(q, t, \Delta P)$. Fig. 4 shows the signal matrix with dimension 32×128 , where the instance in time t is chosen to show only the spin echo centers. The coherence pathway spectrum

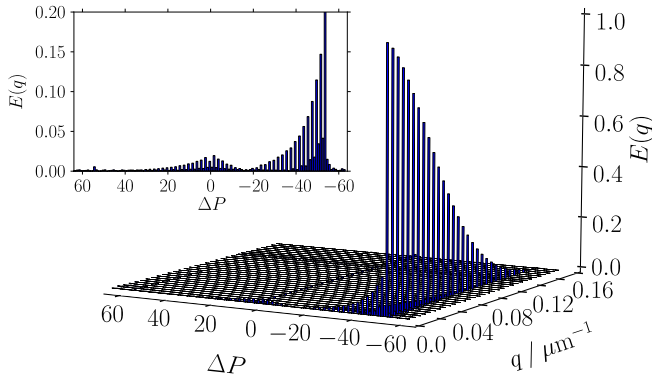


Figure 4: Coherence transfer pathway map obtained by applying MRPI including the PIETA phase cycling scheme to the spherical water sample. Shown is the real part of signal matrix at the center of the spin echo as a function of the cumulative coherence change ΔP . The desired pathway is the direct coherence pathway with $\Delta P = -54$. The inset shows the CP spectrum for zero pulsed field gradient amplitude ($q = 0$).

shows several peaks in the ΔP dimension for the first row in the spectrum where $q = 0$. Since the contribution of unwanted pathways is the highest for zero gradient amplitude the corresponding ΔP spectrum is shown separately in the inset. The direct coherence pathway can be selected at $\Delta P = -54$ according to eq. 10. It is apparent that the attenuation of the pathway with $\Delta P = -54$ follows a Gaussian shape as expected by eq. 16, while all other pathways experience a sharper drop in amplitude when q is increased. This is a consequence of their dephasing with increasing gradient pulse amplitudes. One exception being the CP at $\Delta P = 0$, with $\vec{p} = (0, +1, 0, \dots, 0, -1)$. This CP is not dephased, since it is only influenced by the constant read gradient in the beginning and the end of the pulse sequence G_R for which the spin echo condition $\int_0^T G_R^*(t) dt = 0$ is full-filled

regardless of the amplitude of the other pulsed gradients. This pathway was accounted for when designing the 4-step phase cycling scheme discussed in sec. 3.1. Furthermore, the relative amplitude of all signal contributions at low q values is high enough to significantly impact on the spin echo amplitude if they are not filtered in an experiment without PIETA. The most important pathways are the ones close to $\Delta P = 0$, which are stimulated echo pathways with many intervals where the magnetization is stored in the z -direction (i.e. many elements with $p_k = 0$), while coherence pathways close to the direct pathway with $\Delta P = -54$ also appear with significant intensity. The latter pathways are characterized by a small number of time intervals where the magnetization is stored in z -direction. During the z -storage time intervals the magnetization associated with these CPs is subject to T_1 relaxation instead of T_2 relaxation. Thus, their relative amplitude with respect to the direct CP may be very high even in the case of nearly perfect rotations of the magnetization.

Fig. 5 shows the normalized spin-echo attenuation $E(q)$ as obtained by selecting the direct coherence pathway with $\Delta P = -54$ (squares) in comparison to an MRPI experiment performed with the 4-step phase cycle (triangles). All parameters were

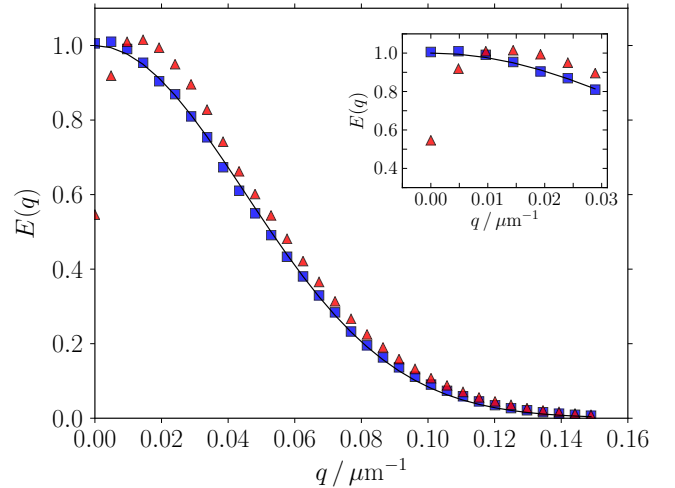


Figure 5: Comparison of the MRPI spin echo attenuation between the 4-step phase cycling scheme (triangles) and the PIETA phase cycling scheme with subsequent selection of the direct coherence pathway (squares). The insert shows a zoom of the signal amplitudes at low q values.

kept the same for both experiments except for the phase cycling scheme. For both experiments the gradient duration was $\delta' = 2 \text{ ms}$ and the inter 180° rf-pulse spacing was $2\tau = 2.5 \text{ ms}$. The solid line in fig. 5 represents the fit of the experimental data against eq. 16. The fitted self-diffusion coefficient was $D = (2.8 \pm 0.2) \times 10^{-9} \text{ m}^2 \text{ s}^{-1}$, which is higher than the literature value for $T = 293 \text{ K}$ of $D = (2.0 \pm 0.2) \times 10^{-9} \text{ m}^2 \text{ s}^{-1}$ [32]. However, it has been shown that the right self-diffusion coefficient can be obtained with MRPI when less gradient pulses are utilized [8]. This suggests that the gradient ramp times which are not accounted for in eq. 18 may play an increasingly important role with increasing numbers of gradient pulses. This is consistent with findings for pulse sequences specifically de-

signed for the measurement of self-diffusion coefficients [33].

Nonetheless, the expected Gaussian attenuation is obtained and the effect of the coherence pathways on the spin echo amplitude for low q values can be studied. Clearly, the amplitudes of the first four data points are lower than expected for the 4-step phase cycle (triangles). Especially the first point measured with zero gradient amplitude is 45% below the expected amplitude. This signal suppression is caused by spurious coherence pathways which interfere with the direct coherence pathway destructively. It may appear surprising that the spin echo amplitude first increases before it asymptotically follows the expected Gaussian attenuation according to eq. 16. This surprising increase in amplitude is caused by the fact that the recorded amplitude is obtained by the sum of the individual CPs. Each CP is associated with a corresponding complex magnetization. When the magnetization of the CPs is recorded with a different magnetization phase during detection, they do interfere destructively. On the other hand, the spin echo attenuation extracted from the MRPI PIETA experiment does not suffer from destructive interference and thus the correct amplitude for low q -values was recovered.

Following the bulk experiments, MRPI PIETA was applied to the capillary sample with the gradient pulses applied perpendicular to the cylinder axis. The number of long gradient pulses was $N_L = 30$ and therefore $n_E = 33$.

The number of phase steps was set to $N = 64$, which was 2 phase steps less than required by eq. 11. This was due to the requirement of FFT algorithms to operate on sampling points of multiples of power of two, else the necessary number of phase steps would have been $N = 128$. This would have extended the experimental time beyond practical limits. In hindsight, a Bluestein algorithm [34] accepting an arbitrary number of samples would be favorable in the future. Analysis of the results, however, can still be carried out with the under sampled data set, since fold-back signals do not overlap in the resulting coherence pathway spectrum. Fig. 6 shows the real part of the matrix $s(q, \Delta P)$ with the dimension 16×64 , which was obtained from the matrix $s(q, t, \Delta P)$ by selecting the signal at the time instance of the spin echo center. Further parameters were the gradient duration of $\delta' = 4.635$ ms and the echo time of $2\tau = 5.56$ ms. Due to the under sampling of the spectrum in the ΔP dimension, one obtains a CP spectrum with fold backs of the desired signal $\Delta P = -34$ which appears at $\Delta P = 30$. Similar to the experiment shown for the free self-diffusion case there are several coherence pathways close to $\Delta P = -32$ and in the centre of the spectrum at $\Delta P = 0$ for $q = 0$. Here, however also CPs close to $\Delta P = +32$ are contributing significantly. These pathways are initially following the pathway $\mathbf{p} = (0, -1, +1, \dots, -1)$ which is conjugate to the desired pathway $\tilde{\mathbf{p}} = (0, +1, -1, \dots, -1)$ and they are transferred with the last few 180° rf-pulses into coherence pathways which are detectable. These CPs appear in the cylindrical capillary spectrum, while they do not contribute appreciably to the bulk H_2O spectrum shown in fig. 4. This may be explained by higher internal gradients in the capillaries which render the rf-pulse rotations less ideal than in the bulk sample. Thus, the contributions of coherence pathways depends on the sample as well

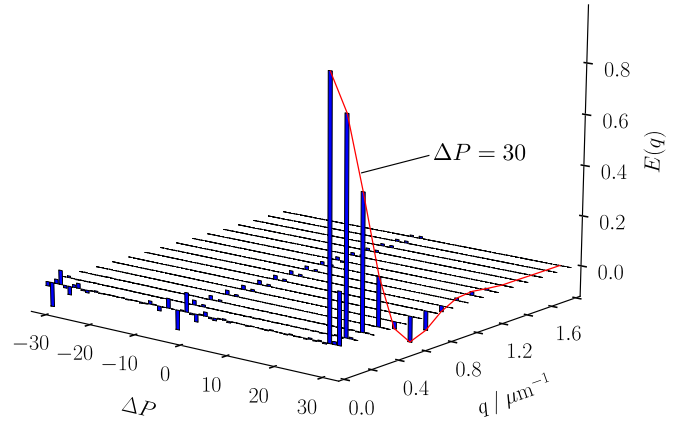


Figure 6: Coherence transfer pathway map obtained by applying MRPI including the PIETA phase cycling scheme to the cylindrical capillary sample. Real part of the coherence pathways with total coherence change ΔP for the center of the spin echo. The desired pathway is the direct coherence pathway with $\Delta P = -34$ which appears at $\Delta P = 30$ due to fold-back.

as the careful adjustment of the rf-pulse durations. Regardless, their relative importance can be measured directly with PIETA and the desired coherence pathway can be extracted.

Figure 7 (squares) shows the real part of the signal as obtained by selecting the direct coherence pathway appearing at $\Delta P = 30$. The spin echo amplitude for the 4-step phase cycle

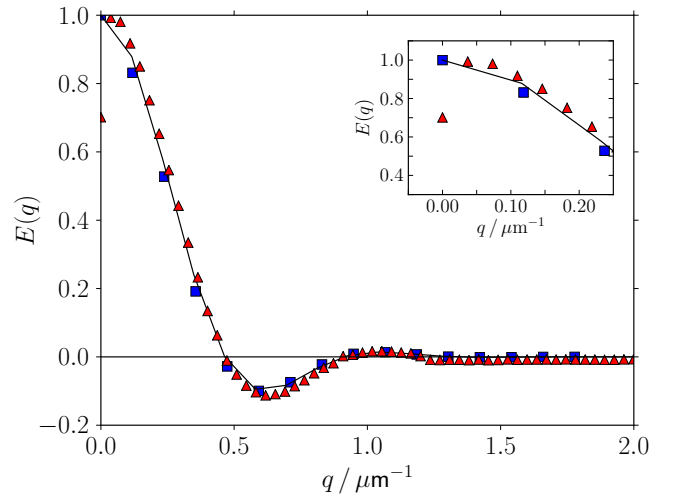


Figure 7: Real part of the q -space profile of the capillary sample as obtained by the MRPI pulse sequence. The spin echo amplitude for the experiment utilizing the 4-step phase cycle (triangles) is distorted at low gradient strengths due to destructive coherence pathways. The solid line was obtained by MCF simulation [8]. The insert shows a zoom of the signal amplitudes at low q values.

(triangles) is suppressed by 30% below the expected amplitude at zero gradient strength ($q = 0$). The q -values in this experiment are over a factor of 10 larger than in the experiments with the bulk H_2O sample shown in fig. 5. Therefore, only the first and second data points are affected by the destructive coherence pathways, while for all the following q -steps these CPs have been dephased. Furthermore, the number of 180° rf-pulses is

only $n_{180} = 33$ versus $n_{180} = 53$ in the bulk experiments shown in fig. 5. Thus, the relative importance of undesired coherence pathways to the desired coherence pathway is higher in experiments with more rf-pulses.

The solid line in fig. 7 is the simulated signal as obtained with the Multiple Correlation Function technique [8]. The signal extracted from the PIETA experiment recovers the signal amplitudes for low values of q . Furthermore, the signal phase is preserved with this phase cycling technique as can be seen by the positive and negative lobes in fig. 7. Thus, PIETA may not only prove useful for relaxation studies in CPMG like experiments, but it can also help with the development of imaging techniques where phase preservation through a sequence of 180° rf-pulses is a major concern. Such techniques are for example Rapid Imaging with Refocused Echoes (RARE) experiments [35] and spatially resolved T_2 experiments [36].

5. Conclusions

It has been shown that PIETA can recover the desired NMR signal in cases where a broad coherence pathway spectrum complicates the design of complete phase cycles with the nested phase cycling approach. The results with MRPI PIETA show that the NMR signal phase due to gradient pulses can be preserved with this phase cycling technique, which may prove beneficial for applications involving other NMR imaging techniques. The only two steps required for implementing PIETA are to cycle every second rf-pulse phase and to respect the Nyquist-Shannon criterion for the number of phase increments recorded. This standardized scheme of implementation may shorten the time required for pulse sequence design by allowing one to extract the desired signal without a deep analysis of the CP spectrum. However, PIETA requires an extra Fourier transform processing step as compared to Cogwheel phase cycling. Thus, Cogwheel phase cycling may be more efficient during routine application of pulse sequences where the extra information about contributing coherence pathways is not needed. Prime candidates for applications of PIETA are CPMG like pulse sequences. Such pulse sequence designs are increasingly utilized for a broad range of NMR experiments. Examples involving spin-1/2 nuclei include the spectral characterization of the self-diffusion of molecules [37], compartment sizing in MRI [38] and the enhancement of the signal in low field NMR. It can be assumed that the PIETA approach will prove beneficial for these applications in the future.

Acknowledgements

We gratefully acknowledge financial support by the Ministry of Business, Innovation and Employment of New Zealand. S.H. thanks Victoria University of Wellington for receiving support through a Ph.D. scholarship.

References

- [1] E. O. Stejskal, J. E. Tanner, Spin diffusion measurements: Spin echoes in the presence of a time-dependent field gradient, *J. Chem. Phys.* 42 (1965) 288–292.
- [2] P. T. Callaghan, *Translational Dynamics & Magnetic Resonance*, Oxford University Press, Oxford, 2011.
- [3] P. T. Callaghan, A. Coy, D. Macgowan, K. J. Packer, F. O. Zelaya, Diffraction-like effects in NMR diffusion studies of fluids in porous solids, *Nature* 351 (1991) 467.
- [4] F. B. Laun, T. A. Kuder, W. Semmler, B. Stieltjes, Determination of the defining boundary in nuclear magnetic resonance diffusion experiments, *Phys. Rev. Lett.* 107 (2011) 048102.
- [5] F. B. Laun, T. A. Kuder, A. Wetscherek, B. Stieltjes, W. Semmler, NMR-based diffusion pore imaging, *Phys. Rev. E* 86 (2012) 021906.
- [6] T. A. Kuder, P. Bachert, J. Windschuh, F. B. Laun, Diffusion pore imaging by hyperpolarized xenon-129 nuclear magnetic resonance, *Phys. Rev. Lett.* 111 (2013) 028101.
- [7] S. Hertel, M. Hunter, P. Galvosas, Magnetic resonance pore imaging, a tool for porous media research, *Phys. Rev. E* 87 (2013) 030802.
- [8] S. A. Hertel, X. Wang, P. Coard, C. Simpson, M. Hunter, P. Galvosas, Magnetic Resonance Pore Imaging of microscopic non-symmetric pore shapes, *Phys. Rev. E* 92 (2015) 012808.
- [9] G. Goelman, M. Prammer, The CPMG pulse sequence in strong magnetic field gradients with applications to oil-well logging, *J. Magn. Reson. A* 113 (1995) 11 – 18.
- [10] M. D. Hürlimann, Diffusion and relaxation effects in general stray field NMR experiments, *J. Magn. Reson.* 148 (2001) 367–378.
- [11] Y. Q. Song, Categories of coherence pathways for the CPMG sequence, *J. Magn. Reson.* 157 (2002) 82–91.
- [12] J. H. Baltisberger, B. J. Walder, E. G. Keeler, D. C. Kaseman, K. J. Sanders, P. J. Grandinetti, Phase incremented echo train acquisition in NMR spectroscopy, *J. Chem. Phys.* 136 (2012) 211104.
- [13] M. H. Levitt, *Spin dynamics: Basics of Nuclear Magnetic Resonance*, Wiley, 2001.
- [14] A. D. Bain, Coherence levels and coherence pathways in NMR. A simple way to design phase cycling procedures, *J. Magn. Reson.* 1969 56 (1984) 418 – 427.
- [15] G. Bodenhausen, H. Kogler, R. Ernst, Selection of coherence-transfer pathways in NMR pulse experiments, *J. Magn. Reson.* 1969 58 (1984) 370 – 388.
- [16] C. E. Hughes, M. Carravetta, M. H. Levitt, Some conjectures for cogwheel phase cycling, *J. Magn. Reson.* 167 (2004) 259 – 265.
- [17] A. Jerschow, N. Müller, Efficient simulation of coherence transfer pathway selection by phase cycling and pulsed field gradients in NMR, *J. Magn. Reson.* 134 (1998) 17 – 29.
- [18] J. Ollerenshaw, R. McClung, Construction of phase cycles of minimum cycle length: MakeCycle, *J. Magn. Reson.* 143 (2000) 255 – 265.
- [19] R. E. D. McClung, Coherence transfer pathways and phase cycles: The decoding of a pulse sequence, *Conc. Magn. Reson.* 11 (1999) 1–28.
- [20] M. H. Levitt, R. Freeman, NMR population inversion using a composite pulse, *J. Magn. Reson.* (1969) 33 (1979) 473 – 476.
- [21] A. Bax, P. De Jong, A. Mehlkopf, J. Smidt, Separation of the different orders of NMR multiple-quantum transitions by the use of pulsed field gradients, *Chem. Phys. Lett.* 69 (1980) 567–570.
- [22] H. Y. Carr, E. M. Purcell, Effects of diffusion on free precession in nuclear magnetic resonance experiments, *Phys. Rev.* 94 (1954) 630–638.
- [23] S. Meiboom, D. Gill, Modified spin-echo method for measuring nuclear relaxation times, *Rev. Sci. Instrum.* 29 (1958) 688–691.
- [24] M. H. Levitt, P. Madhu, C. E. Hughes, Cogwheel phase cycling, *J. Magn. Reson.* 155 (2002) 300 – 306.
- [25] R. R. Ernst, G. Bodenhausen, A. Wokaun, *Principles of Nuclear Magnetic Resonance in One and Two Dimensions*, Clarendon Press, Oxford, 1987.
- [26] N. Ivchenko, C. E. Hughes, M. H. Levitt, Multiplex phase cycling, *J. Magn. Reson.* 160 (2003) 52 – 58.
- [27] G. Drobny, A. Pines, S. Sinton, D. P. Weitekamp, D. Wemmer, Fourier transform multiple quantum nuclear magnetic resonance, *Faraday Symp. Chem. Soc.* 13 (1978) 49–55.
- [28] B. J. Walder, K. K. Dey, D. C. Kaseman, J. H. Baltisberger, P. J. Grandinetti, Sideband separation experiments in NMR with phase incremented echo train acquisition, *J. Chem. Phys.* 138 (2013).

- [29] C. E. Shannon, Communication in the presence of noise, Proc. Institute of Radio Engineers 37 (1949) 10–12.
- [30] D. S. Grebenkov, NMR survey of reflected Brownian motion, Rev. Mod. Phys. 79 (2007) 1077–1137.
- [31] F. Stallmach, P. Galvosas, Spin echo NMR diffusion studies, in: Annu. Rep. NMR Spectrosc., volume 61, Elsevier, Amsterdam, Boston, Heidelberg, 2007, pp. 51–131.
- [32] M. Holz, S. R. Heil, A. Sacco, Temperature dependent self-diffusion coefficients of water and six selected molecular liquids for calibration in accurate ^1H NMR PFG-measurements, Phys. Chem. Chem. Phys. 2 (2000) 4740.
- [33] W. S. Price, P. W. Kuchel, Effect of nonrectangular field gradient pulses in the Stejskal and Tanner (diffusion) pulse sequence, J. Magn. Reson. 94 (1991) 133–139.
- [34] L. Bluestein, A linear filtering approach to the computation of discrete fourier transform, IEEE Transactions on Audio and Electroacoustics 18 (1970) 451–455.
- [35] J. Hennig, A. Nauerth, H. Friedburg, RARE imaging: A fast imaging method for clinical MR, Magn. Reson. Med. 3 (1986) 823–833.
- [36] L. Li, H. Han, B. J. Balcom, Spin echo SPI methods for quantitative analysis of fluids in porous media, J. Magn. Reson. 198 (2009) 252 – 260.
- [37] P. T. Callaghan, J. Stepisnik, Frequency-domain analysis of spin motion using modulated-gradient NMR, J. Magn. Reson. A 117 (1995) 118–122.
- [38] N. Shemesh, G. A. Álvarez, L. Frydman, Measuring small compartment dimensions by probing diffusion dynamics via non-uniform oscillating-gradient spin-echo (NOGSE) NMR, J. Magn. Reson. 237 (2013) 49 – 62.